Article

pubs.acs.org/Biomac

Transparent Films Based on PLA and Montmorillonite with Tunable Oxygen Barrier Properties

Anna J. Svagan,*[,†] Anna Åkesson,[‡] Marité Cárdenas,[‡] Sanja Bulut,[§] Jes C. Knudsen,[†] Jens Risbo,[†] and David Plackett[∥]

[†]Department of Food Science, University of Copenhagen, Rolighedsvej 30, DK-1958 Frederiksberg C, Denmark

[‡]Department of Chemistry and NanoScience Center, University of Copenhagen, Universitetsparken 5, DK-2100 Copenhagen, Denmark

[§]Department of Micro- and Nanotechnology, Technical University of Denmark, Ørsteds plads, DK-2800 Kgs. Lyngby, Denmark

[∥]Department of Chemical and Biochemical Engineering, Technical University of Denmark, Soltofts plads, DK-2800 Kgs. Lyngby, Denmark

ABSTRACT: Polylactide (PLA) is viewed as a potential material to replace synthetic plastics (e.g., poly(ethylene terephthalate) (PET)) in food packaging, and there have been a number of developments in this direction. However, for PLA to be competitive in more demanding uses such as the packaging of oxygen-sensitive foods, the oxygen permeability coefficient (OP) needs to be reduced by a factor of ∼10. To achieve this, a layer-by-layer (Lbl) approach was used to assemble alternating layers of montmorillonite clay and chitosan on extruded PLA film surfaces. When 70 bilayers were applied, the OP was reduced by 99 and 96%, respectively, at 20 and 50% RH. These are, to our knowledge, the best improvements in oxygen barrier properties ever reported for a PLA/clay-based film. The process of assembling such multilayer structures was characterized using a quartz crystal microbalance with dissipation monitoring. Transmission electron microscopy revealed a well-ordered laminar structure in the deposited multilayer coatings, and light transmittance results demonstrated the high optical clarity of the coated PLA films.

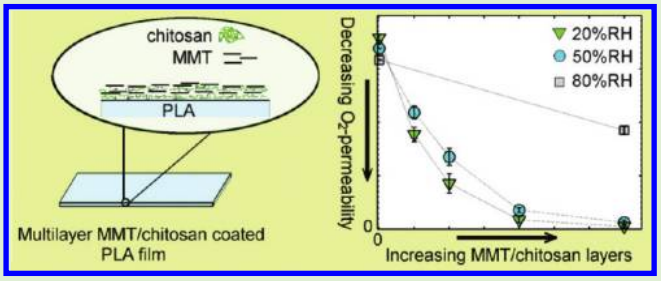

INTRODUCTION

Today's growing awareness of sustainability has shifted the focus from conventional plastic materials to more environmentally friendly alternatives in different fields of application including food packaging. As such, the potential of polylactide (PLA) as a sustainable replacement for traditional petrochemical-derived polymers in packaging applications has received much attention.[1] PLA is a biodegradable thermoplastic that can be produced from agricultural resources and has acceptable physical, mechanical and gas barrier properties for some uses.[2,3] However, much effort is still needed to enhance the properties of PLA so as to make it competitive with petroleum-based plastics in demanding applications, such as the packaging of oxygen-sensitive foods. For instance, the oxygen permeability (OP) coefficient of PLA needs to be reduced by a factor of ∼10 before it can compete with PET, a conventional plastic commonly used for this purpose.[3] A number of approaches have been investigated to improve the gas barrier properties of PLA,[4−6] the most popular being the inclusion of impermeable layered silicate clays.[7−9] For this purpose, a variety of processing strategies, including melt extrusion, in situ polymerization, and solvent casting, have been explored.[8−10] When processing conditions are optimized, the use of nanoclay can provide an enhancement in gas barrier properties due to the formation of a tortuous diffusion path. To attain such improvement, it is desirable to maximize the aspect ratio of the clay platelets, which can be achieved once the nanoclay is well-dispersed and exfoliated in the polymer matrix, and to orient each clay platelet's largest dimension perpendicular to the direction of the diffusion path.[11] However, when using conventional processing techniques, complete exfoliation and orientation of nanoclays is a challenging task and, as a result, PLA-clay nanocomposites typically show at most ∼60% reduction in OP (0% RH, 23−25 °C).[8,9] This reduction is usually observed at low clay contents of ∼5−10 wt %, whereas at higher loadings, clay platelets tend to aggregate, which may marginally increase or even reduce the barrier properties.[12,13]

Recently, an alternative strategy using a bottom-up layer-by-layer (Lbl) process has been employed to assemble clay based nanocomposites.[14−17] In this case, free-standing films consisting of hundreds of alternating, electrostatically self-assembled layers of clay and polymer are constructed by sequential adsorption of oppositely charged clay and polymer. The resulting multilayer films contain a well-defined "brick-wall"

Received: October 13, 2011
Revised: December 13, 2011
Published: January 9, 2012

architecture consisting mainly of single (exfoliated) clay platelets sandwiched between polymer layers that are a few nanometers in thickness.[15] The volume fraction of nanoclay can easily be modified[18] and scales with the gas barrier properties provided that the free volume of the polymer layers remains low.[11,19,20] Using the Lbl approach, it is also possible to create multilayer coatings, and, from the perspective of packaging applications, coatings are more appealing than multilayer films because they require less time to assemble. Grunlan et al.[21−23] used the Lbl technique to create a multilayer coating consisting of a few layers of negatively charged montmorillonite (MMT) clay and cationic polyethylenimine (PEI) or polyacrylamide (PAM) on a PET film. The result was a marked increase in oxygen barrier properties. These coated PET films may, however, not be ideal for food packaging applications because acrylamide monomer, which can be present in residual amounts in PAM and released from the polymer under environmental conditions, is a suspected carcinogen and a cumulative neurotoxin, and PEI is reported to be cytotoxic.[24,25] There might also be a risk to human health associated with the presence of MMT clay in food packaging, however, results from a recent report have shown MMT clay not to be cytotoxic.[26] Still, as a precaution, migration of clay from the multilayer coating to food should be avoided by limiting direct contact, for example, by use of a protective coating on top of the multilayer structure. An additional coating could also protect the clay-based multilayer coating from possible wear and the packaged food products from any changes in taste/smell due to the presence of the multilayer coating.

Herein, the Lbl technique was exploited in the creation of novel multilayer-coated PLA films using the polycation chitosan as a bioderived, antibacterial, and nontoxic alternative to the above-mentioned cationic polyelectrolytes.[27] The primary goal was to improve significantly the oxygen barrier of PLA for it to compete with PET in food packaging application such as food trays intended for modified atmosphere packaging. In this respect, improvements in water vapor barrier properties were also of interest. To understand better the effective Lbl deposition process, quartz crystal microbalance with dissipation (QCM-D) monitoring was used to study the formation of two multilayer systems: PLA/MMT and MMT/chitosan. To improve clay exfoliation, we subjected MMT suspensions to high-pressure homogenization, and the oxygen permeance of the resulting multilayer coating was studied. The morphology of coated PLA films was characterized using UV/visible transmittance and transmission electron microscopy (TEM).

EXPERIMENTAL DETAILS

Materials. Low-molecular-weight chitosan from crab shells (viscosity = 42 mPa s at 1% w/w in 1% acetic acid solution) and acetonitrile were purchased from Sigma-Aldrich. Glacial acetic acid was obtained from Merck Chemicals. Cloisite Na^+ (MMT) was kindly donated by Southern Clay Products(Gonzalez, TX). Individual MMT platelets are 1 nm thick and ca. 10−1000 nm in diameter and have a reported density of 2.86 g cm^{-3}.[28,29] PLA films were melt extruded at the facilities of the masterbatch manufacturer Kunststof Kemi A/S (Nykøbing, Denmark). The films had a thickness of ca. 500 μm, a typical film thickness used in the production of thermoformed trays for food packaging. The PLA used for melt processing into films and in the QCM-D experiments was Ingeo, 2003D (NatureWorks), which has a $\bar{M}_w$ = 193 000 g mol^{-1} and $\bar{M}_n$ = 114 000 g mol^{-1} as determined by gel permeation chromatography (GPC). Deionized water (18.2 MΩ cm, Milli-Q Academic, Millipore) was used in all experiments.

Preparation of Multilayer-Coated PLA Films. Aqueous suspensions of MMT (0.2 wt %, natural pH ∼9) were prepared by dispersing 2 g of MMT in 1 L of deionized water. The suspensions were magnetically stirred at medium speed for 5 days; then, selected samples were subjected to one or four passages through a EmulsiFlex-C5 high-pressure homogenizer (Avestin, Ottawa, Canada) at 5000 psi. The suspensions were left for 1 day to sediment, and the clear supernatant phase was then collected and used in the experiments. Aqueous solutions of chitosan (0.2 wt %) were prepared by dissolving 2 g of chitosan in 1 L of 0.235% (v/v) acetic acid solution. This solution was magnetically stirred for 4 days. Afterward, the pH was adjusted to 6.0 with 1 M NaOH, and the solution was filtered through filter paper with a pore size of 0.22 μm. The primary amino groups in chitosan are sensitive to the pH of the solution. At pH 6.0, a small fraction of the primary amino groups (pK_a ∼6.4)[15] in chitosan are protonated, making the average polyelectrolyte segment−segment interactions more favorable and the segment−water interaction less favorable.[30] As such, the pH will also affect the multilayer formation during Lbl processing. At pH 6.0, Podsiadlo et al. reported a more regular growth in multilayer thickness during Lbl processing compared with that obtained at lower pH values.[15] A previous study also showed that at pH 6.0 the adsorbed chitosan layer structure will be more compact than that at lower pH values.[30]

MMT/chitosan multilayer structures were created on PLA films using the processing steps depicted in Scheme 1. Prior to deposition, the PLA film was rinsed with water. The film was initially dipped in the chitosan solution for 5 min, followed by rinsing with water for 2 min. The same procedure was followed with the MMT suspension. Afterward, the adsorbed layers were dried under ambient conditions. This gave a single deposition cycle, creating two bilayers of MMT and chitosan, one on each side of the PLA film. Unless otherwise stated, the number of bilayers given for a multilayer-coated PLA film always refers to the sum of bilayers on both sides of the film. In all subsequent steps, 1 min of deposition and rinsing was employed. In an effort to eliminate any influence that the PLA film could have on the Lbl assembly, the counting of the number of bilayers deposited started after the initial three deposition cycles. All coated films were stored for at least 1 week at room temperature in a desiccator containing silica gel drying agent prior to characterization.

Scheme 1. Schematic of the Lbl Deposition Process and a Simplified Out-of-Scale Image of the Resulting Multilayer MMT/Chitosan Structure Deposited on the PLA Films[a]

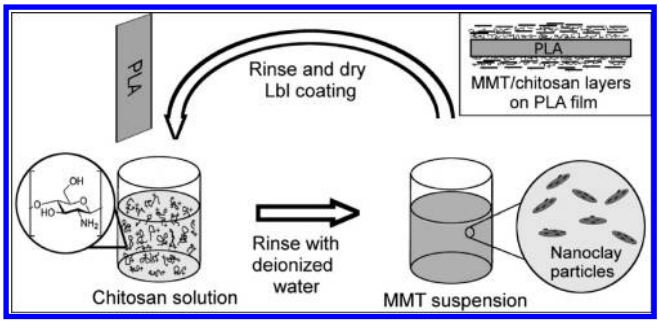

[a]Drying was only employed once per deposition cycle.

Quartz Crystal Microbalance with Dissipation (QCM-D). The bilayer formation on gold-coated crystals was monitored in situ using a QCM-D (E1, Q-Sense AB, Sweden). The build-up of two multilayer structures, MMT/chitosan and MMT/PLA, was studied. QCM-D is a technique that allows monitoring in situ adsorption processes on the millisecond time scale. This technique measures the resonance frequency of a quartz oscillator and its energy dissipation (ratio of dissipated energy to stored energy during one period of oscillation), ΔD, which net values change in response to surface-sensitive processes. The change in resonance frequency, ΔF, is associated with a change in wet mass, whereas the change in dissipation is related

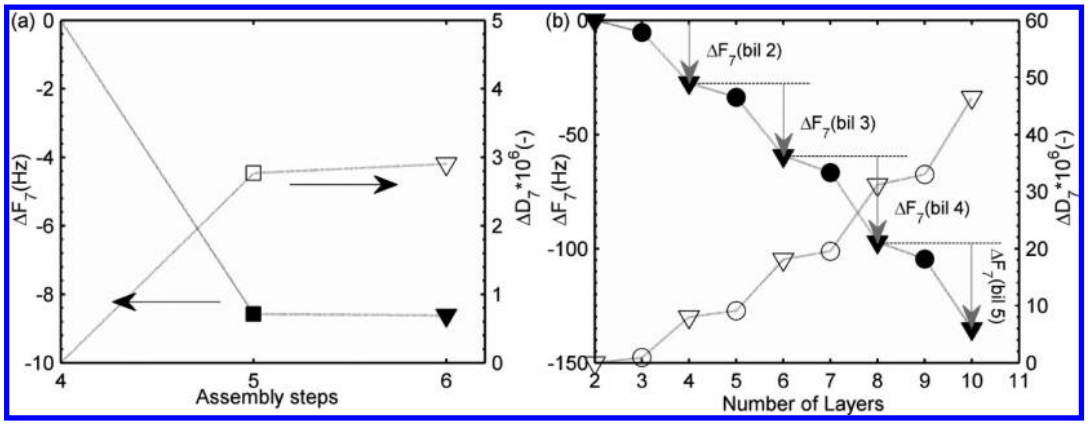

Figure 1. Change in resonance frequency, ΔF_7 (filled symbols), and corresponding energy dissipation change, ΔD_7 (empty symbols), of overtone 7 from QCM-D measurements as functions of the number of adsorbed layers. (a) Attempt to adsorb MMT (▼) onto PLA (■). (b) Successful multilayer formation of chitosan (●) and MMT (▼). Lines are added as guides to the eye.

to the viscoelastic properties of the adsorbed layer.[31] For rigidly and uniform adsorbed layers, the frequency change is directly proportional to the mass oscillating with the crystal, Δm (ng cm^{-2}), as expressed by the Sauerbrey equation.[32]

$$\Delta m = -\Delta F/nC \quad (1)$$

In eq 1, n is the overtone number and C is the mass-sensitive constant, 5.72 m^2 Hz mg^{-1}, for 5 MHz basal shear rate resonance frequency. The gold-coated crystals were cleaned immediately prior to use as follows: (1) UV/ozone treatment for 10 min (UV/ozone Procleaner, BioForce Nanosciences); (2) heating for 5 min at 75 °C in a 5:1:1 mixture of deionized water, ammonia (25%), and hydrogen peroxide (30%); (3) surface rinsing with deionized water and drying with nitrogen gas; and (4) UV/ozone treatment for 10 min. All adsorption experiments were performed in the wet state at a flow rate of 140 μL min^{-1} and at 25 °C. Before and after each MMT and chitosan adsorption stage, a rinsing stage with deionized water was utilized to remove excess material. Before and after each PLA adsorption stage, a rinsing stage with acetonitrile was used. For each adsorption step, sufficient time was allowed to reach a steady-state QCM-D signal. The net change in frequency (or dissipation) per assembly step as plotted in Figure 1 was obtained by taking the difference in the measured frequency (or dissipation) prior to the adsorption stage of wet mass (chitosan, PLA, or MMT) and at the end of the subsequent rinsing stage. The first two to four adsorbed layers closest to the QCM-D crystal were always omitted from the results in Figure 1, given that they depended on the surface properties of the crystal used and were hence not considered representative of the multilayer buildup. The chitosan solution and MMT suspensions were prepared as previously described with the modification that the MMT suspensions were not high-pressure homogenized. The PLA solution (0.1 wt %) was prepared by dissolving PLA in acetonitrile at 65 °C. The selection of acetonitrile as solvent was based on a previous study on multilayer formation of poly(D-lactic acid) and poly(L-lysine).[33]

Dynamic Light Scattering (DLS) and Zeta Potential Measurements. Hydrodynamic diameter and zeta potential measurements on MMT suspensions were performed on a ZetaPALS/BI-MAS apparatus (Brookhaven Instruments). The diode laser in this instrument has nominal raw power of 35 mW and wavelength of 660 nm. The MMT suspensions were prepared, as previously described. The accuracy and repeatability of particle size measurements was ±1 to 2% for monodisperse and dust-free samples. The detectable particle size range was 2 nm to 3 μm. All size measurements were based on 90° angle light scattering. The hydrodynamic diameter was calculated directly by the instrument software using the method of cumulants and a non-negatively constrained least-squares algorithm and application of the Stokes−Einstein equation.[34]

For zeta potential measurements, the ZetaPALS/BI-MAS instrument utilizes a phase analysis light scattering method that is an extension of laser electrophoretic light scattering. In this case, the velocity of a measured particle is the product of electrophoretic mobility and the electric field. Measurements were performed using Plexiglass-based electrodes and at a 15° light scattering angle. Size and zeta potential measurements were performed at 25 °C utilizing a sample volume of 0.5 to 1 mL in disposable acrylic curvets. Two measurements were performed for each suspension type.

Oxygen and Water Vapor Permeability. Oxygen gas transmission rate (OTR) through coated or uncoated PLA films was determined according to ASTM standard F2622-08 using a Lyssy OPT-5000 apparatus (PBI-Dansensor, Denmark). Tests were performed at 23 °C, 101.325 kPa pressure, and 20, 50, or 80% RH. The circular film measuring area was 42 cm^2. Oxygen gas (Alphagaz, Air Liquide Denmark) with a purity of >99.999% was used. The films were conditioned for at least 12 h in the diffusion cell. The time to reach steady-state after introduction of the oxygen gas was <2 h. For each sample, measurements were repeated until four successive readings deviated <5% from the average value, which was then taken as the OTR value. Two specimens were tested for each film type.

Water vapor transmission rate (WVTR) measurements were performed using a Lyssy L80-5000 WVP tester (PBI-Dansensor, Denmark) following ASTM standard E398-03. Tests were performed at 37.9 ± 0.1 °C and at atmosphere pressure. The relative humidity was set to 98% in the wet chamber to avoid condensation and 10% in the dry chamber, yielding a driving force of 88% RH. Calibration was performed with a 19 μm PET film. The circular film measuring area was 50 cm^2. For each sample, measurements were repeated until seven successive readings deviated <5% from the average value, which was then taken as the WVTR value. Two specimens were tested for each film type. The OP coefficients or water vapor permeability coefficients (WVP) were calculated using eq 2.

$$\mathrm{GP} = P_{\mathrm{film}} \times t = \frac{\mathrm{GTR}}{\Delta p} \times t \quad (2)$$

In eq 2, GP is the gas permeability coefficient (OP or WVP), P_{film} is the gas permeance, and t is the sample thickness. The gas permeance is defined as the ratio of the gas transmission rate (GTR) to the difference between the partial pressure of the gas on the two sides of the film, that is, Δp. The sample thickness was calculated as the average of measurements at 12 different film locations using a Mega-Check Pocket Thickness Meter (List-Magentik).

Transmission Electron Microscopy. TEM was performed using a Philips CM100 TEM. Images were obtained at an acceleration voltage of 80 kV. Thin film cross sections were prepared by embedding a piece of PLA film covered with MMT/chitosan bilayers in epoxy resin (Epon) and sectioning thin slices (ca. 50 nm) with a microtome.

Optical Properties. A Cintra 40 ultraviolet−visible (UV−vis) spectrometer (GBC Scientific Equipment, Australia) was used in

transmittance mode to determine the optical properties of films at wavelengths from 200 to 800 nm. A scan speed of 400 nm min^{-1} and a slit width of 2.0 nm were used. Data points were collected every 4.5 nm.

RESULTS AND DISCUSSION

Layer-by-Layer Processing. To better understand the complexation of nanoclay and polymer into multilayer structures, we performed in situ adsorption experiments using QCM-D. First, we investigated the possibility to build multilayer-coated PLA films consisting of PLA and MMT only as a way of omitting the need for an additional polymer in the multilayer coating. From previous reports,[15,21−23] it is clear that a polymer layer in-between MMT layers is needed to promote the Lbl build-up of the multilayer structure. Figure 1a illustrates an attempt to build a multilayer structure consisting of PLA (■) and negatively charged MMT (▼). It represents a typically observed QCM-D result when trying to adsorb MMT onto PLA.

The change in resonance frequency, ΔF_7, and the energy dissipation change, ΔD_7, corresponding to overtone 7 are reported as functions of the number of assembly steps. The experimental results in Figure 1a show that first PLA from a solution in acetonitrile is giving rise to a drop in resonance frequency, and consequently an amount of PLA has been adsorbed. Subsequently, a portion of MMT suspended in water is introduced in the QCM-D cell with no apparent effect on either frequency or dissipation. This shows that MMT cannot be adsorbed on top of the PLA. The finding can be explained by the slightly negatively surface charge of PLA, due to the presence of residual carboxyl groups, that may electrostatically repel the MMT clay.[35] Hence, from the point of building a multilayer coating on a PLA film, it is clear that the presence of a polycation is required as the primary layer on the PLA film. A polymer other than PLA is also needed in-between the MMT layers to build successfully the multilayer structure.

Figure 1b shows the QCM-D results for the multilayer build-up using chitosan solution (●) and MMT suspension (▼). In this case, the decline in resonance frequency per deposition step confirms that MMT is successfully adsorbed onto each underlying chitosan layer and vice versa. In Figure 1b, layer 2 corresponds to an MMT layer, whereas layers 3 and 4 correspond to the successive addition of chitosan and MMT, respectively. For the second (ΔF_7(bil 2) = −27 Hz), third (ΔF_7(bil 3) = −32 Hz), and fourth (ΔF_7(bil 4) = −38 Hz) bilayers, the step in frequency, $|\Delta F_7(\text{bil } x)|$, increased with increasing bilayer number, indicating that as the multilayer is built up it is easier for new material to adsorb. This behavior could arise because there is less influence from the substrate at larger distances, that is, reduced mutual repulsion of the negatively charged QCM Au crystal and MMT. It could also be due to partial intermixing between layers, as seen from studies on chitosan and mucin by Svensson et al.[36] However, for the fourth and fifth deposited bilayers, the change in frequency was almost the same in magnitude (ΔF_7(bil 5) = −38 Hz), suggesting a tendency toward linear mass increase per bilayer. In a previous study, ellipsometry experiments revealed linear growth in thickness per bilayer in thin Lbl-assembled chitosan/MMT films.[15]

As shown in Figure 1b, the change in frequency is associated with a simultaneous increase in dissipation value. The fairly large step in dissipation value when compared with the frequency change per adsorbed layer ($\Delta D_7 > 1 \times 10^{-6}$ per 10 Hz) suggests that the multilayer structure does not respond elastically with the oscillating stress.[37] This result is in agreement with the large divergence in magnitude observed for both frequency and dissipation values for the various QCM-D overtones (not shown). The multilayer can be envisioned as an accordion with low (chitosan) and high (MMT) density layers, for which the QCM-D signal is dominated by viscoelastic properties upon shearing. The result is that the relationship most frequently used to convert the resonance frequency change to mass (i.e., the Sauerbrey equation) will underestimate the mass adsorbed.[32] Aulin et al. studied the Lbl assembly of PEI/microfibrillated cellulose and successfully applied the Johannsmanns model to estimate the correct wet mass from the adsorbed layers.[38] However, for comparative purposes, the Sauerbrey equation can still be applied to the resonance frequency shifts of overtone 7, which shows that, on average, 120 and 490 ng cm^{-2} of hydrated chitosan and hydrated MMT, respectively, are deposited at each layer addition. If the adsorbed layers of chitosan (Δm = 120 ng cm^{-2}) in the QCM-D experiments contain very little water and a density of 1.4 g cm^{-3} is assumed for dry chitosan,[39] then the thickness of each deposited chitosan layer should be ∼1 nm. MMT has a reported density of 2.86 g cm^{-3}, and single dehydrated clay platelets have a thickness of ∼1 nm.[29] Therefore, if one assumes that MMT forms hydrates with three or four pseudolayers of water molecules, that is, a ∼ 1 nm thick water film, then the mass of one continuous layer of hydrated, single MMT platelets should be 440 ng cm^{-2}.[40,41] Hence the value of 490 ng cm^{-2} per MMT adsorption step obtained from the experimental data and the Sauerbrey equation suggests that, on average, at least ∼1 nm thick layer (dehydrated) of clay platelets was successfully adsorbed onto chitosan. The exact layer structure cannot be defined on the basis of QCM-D data, but the MMT platelets are probably not tightly packed on the QCM crystal surface due to geometrical restrictions and their inherent stiffness. There might also be some MMT aggregates (incomplete exfoliation) present as well as partial penetration of MMT platelets into the chitosan layer.

On the basis of the above interpretation of the QCM-D data, the MMT content is estimated to be ca.70 wt % for the whole deposited multilayer structure. This value is close to the value of 80 wt % determined using thermogravimetric analysis in a recent study on free-standing MMT/chitosan films prepared by Lbl.[15] In general, when high MMT content coatings containing single (exfoliated) MMT platelets are targeted, then the polymer layers between the MMT platelets should be made a few nanometers in thickness.[29] The importance of the polymer layer thickness rests on the remarkably high specific surface area, $\hat{S}$, of exfoliated MMT ($\hat{S}$ = 700 m^2 g^{-1}).[29] The QCM-D results in Figure 1b and results by Podsiadlo et al. on free-standing MMT/chitosan films prepared by Lbl[15] show that the Lbl technique can provide very thin layers of chitosan under the given processing conditions. This observation can be compared with the less well-defined nanocomposite structures obtained with conventional processing techniques, such as melt extrusion, in which the orientation of clay and the thickness of the interstitial polymer regions between clay platelets are less easy to control.[8−10]

To obtain optimal barrier properties in clay-based multilayer coatings or nanocomposites, it is important to maximize the aspect ratio of the clay platelets through complete clay exfoliation.[42] In the Lbl technique discussed here, the MMT was suspended in water. Although water has the ability to

delaminate the MMT into individual silicate layers to some extent, larger aggregates are also present.[15,23,40] In fact, previous studies by Podsiadlo et al.[15] showed that some of the MMT, present in Lbl-processed films, was composed of several-sheet-thick stacks. As a result of the reported findings, we directed effort toward improving the delamination of clay in water prior to Lbl processing. Herein, MMT delamination was facilitated by four passages through a high-pressure homogenizer. Measured zeta potentials for MMT suspensions used in the experiments were less than −50 mV, suggesting that the MMT platelets were sufficiently charged to provide a stable state, in which the platelets would not easily aggregate. In Figure 2, DLS

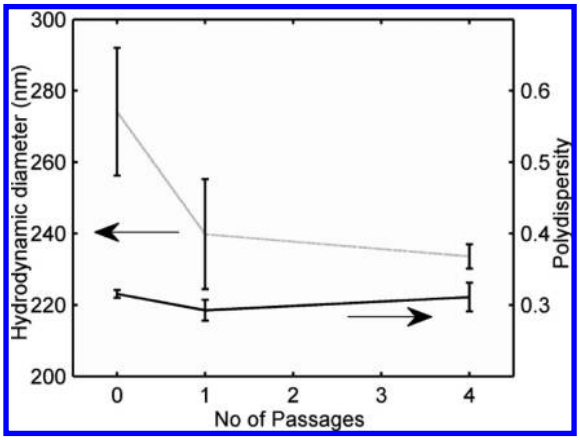

Figure 2. Hydrodynamic diameter and polydispersity of MMT platelets in 0.2 wt % suspension as functions of the number of passages through a high-pressure homogenizer. Lines are added as guides to the eye.

results are presented for homogenized and nonhomogenized MMT suspensions. Results for one passage through the high-pressure homogenizer are included for comparative purposes.

DLS was used as a fast screening tool to evaluate the influence of high-pressure homogenization on the average MMT platelet size.[29] DLS experiments give the hydrodynamic diameter of a spherical particle with the same mobility as the measured particle. Results from DLS showed that the average size was sharply lowered after one passage through the high-pressure homogenizer, followed by a less rapid decrease after four passages. The reported decrease in hydrodynamic diameter after both one and four passages is likely a combination of reduction in platelet area and the delamination of platelet stacks. However, the fact that only a small further reduction in the hydrodynamic diameter is observed once one passage has been performed might indicate that delamination is the governing mechanism after four passages. Significant reduction in platelet area is undesirable because this could potentially lower the barrier properties of the multilayer coating. The polydispersity values, which are dimensionless measures of the broadness of the particle size distributions, implied disperse particle size systems. The results showed that the polydispersity values were not significantly affected by homogenization even after four passages.

To evaluate further the effect of homogenization, we measured the oxygen transmission rates of the resulting multilayer-coated films at 20% RH and 23 °C. The oxygen permeance of the multilayer coating, P_{Lbl}, was calculated from the permeance of the multilayer-coated PLA film, P_{comp}, and that of the neat PLA film, P_{PLA}[43]

$$P_{Lbl} = \left(\frac{1}{P_{comp}} - \frac{1}{P_{PLA}} \right)^{-1} \quad (3)$$

In eq 3, $P_{PLA} = OP_{PLA}/t_{PLA}$, $OP_{PLA} = 17.68 \times 10^{-2}$ mL mm m^{-2} day^{-1} kPa^{-1}, and t_{PLA} are the thickness of the PLA film. The OP_{PLA} value was determined experimentally in the present study.

The data in Figure 3 represent oxygen permeance values of different multilayer coatings prepared using MMT suspensions

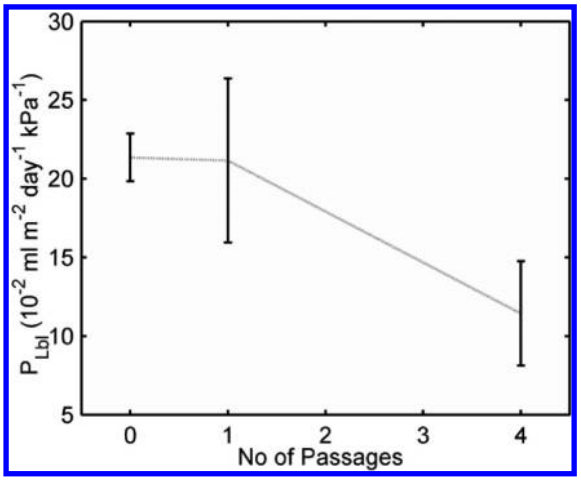

Figure 3. Oxygen permeance at 20% RH and 23 °C of multilayer coatings consisting of 20 bilayers of chitosan/MMT as a function of the number of homogenization steps for the MMT suspensions. Lines are added as guides to the eye.

that were either homogenized or nonhomogenized. All multilayer coatings consisted of 20 bilayers. Interestingly, an improved oxygen barrier was obtained when the MMT suspension was subjected to four passages through the high-pressure homogenizer. As shown in Figure 3, the average oxygen permeance of the multilayer was reduced to almost half the value achieved for the nonhomogenized reference sample (only magnetic mixing). This result is consistent with enhanced delamination of clay stacks as a consequence of homogenization under the given processing conditions. For comparison, results after one homogenization are also included, but in this case no significant improvement can be seen when compared with the nonhomogenized reference. For this reason, MMT suspensions subjected to four passages through the homogenizer were chosen for the study of the morphology, opacity and gas barrier properties of multilayer-coated PLA films.

Morphology of Multilayer-Coated PLA Films. Cross sections of multilayer-coated PLA films were examined using TEM. In Figure 4a,b, the TEM photomicrographs show 20 bilayers of MMT/chitosan deposited on one side of a PLA film at two different magnifications.

In Figure 4b, in particular, the MMT platelets can be seen as dark lines in a laminar structure similar to structures previously observed.[15] This structure emphasizes the high level of clay orientation, with the majority of platelets lying parallel to the PLA film. In Figure 4a, the thickness of the multilayer was estimated to be 205 nm on average, making it almost five times thicker than a similar coating based on QCM-D results (~45 nm, assuming linear mass increase). This finding might be

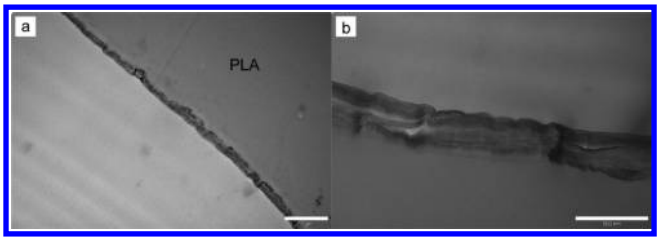

Figure 4. TEM cross-sectional images at two different magnifications showing 20 bilayers of MMT and chitosan on a PLA film. The scale bars are 1 μm (a) and 500 nm (b).

explained by the underestimation used in calculations of the QCM-D data, that is, using the Sauerbrey equation, as previously discussed.

A further advantage of using the Lbl process to apply multilayer structures on PLA films is that the optical clarity remains very close to that of the neat PLA film, with only a slight decrease in transmittance with the increasing number of bilayers (Figure 5).

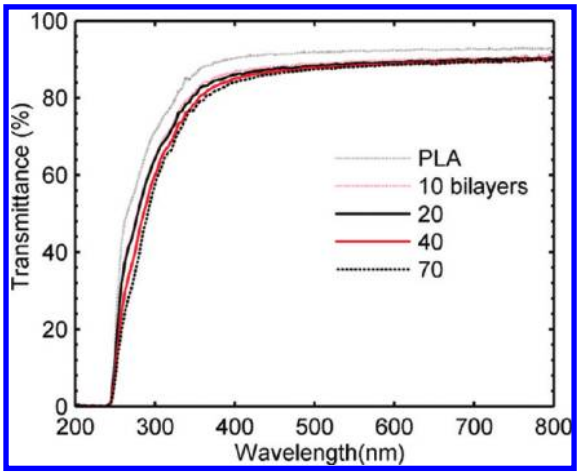

Figure 5. Light transmittance results for neat PLA film and PLA films coated with 10, 20, 40, or 70 MMT/chitosan bilayers. The thickness was ~500 μm for all films.

For example, the light transmittance at 600 nm for neat PLA was 92.4%, whereas the transmittance of PLA films with multilayer coatings was 88.6 to 89.8%. In comparison, conventional melt-processed, clay-filled polymer films are typically much more opaque due to a combination of higher clay addition levels and poor clay exfoliation.[22]

Gas Barrier Properties. The oxygen barrier properties of the multilayer-coated PLA films are presented in Figure 6. In panel a, the OP coefficient is reported for Lbl coated PLA films at 20, 50 or 80% RH. The number of bilayers was varied from 10 to 70.

A very significant decrease in OP was observed with increasing numbers of bilayers at 20 and 50% RH. At 70 bilayers and 20% RH, the average OP value was as low as 0.255 $\times$ 10^{-2} mL mm m^{-2} day^{-1} kPa^{-1}, which is almost two orders of magnitude lower than that of the neat PLA film (17.68 $\times$ 10^{-2} mL mm m^{-2} day^{-1} kPa^{-1}). At 50% RH, the OP increased slightly to 0.635 $\times$ 10^{-2} mL mm m^{-2} day^{-1} kPa^{-1}, a value still much below that of neat PLA film (16.70 $\times$ 10^{-2} mL mm m^{-2} day^{-1} kPa^{-1}). These are, to our knowledge, the lowest OP values ever reported for a PLA/clay-based film. For comparison, conventional PLA/clay nanocomposites typically

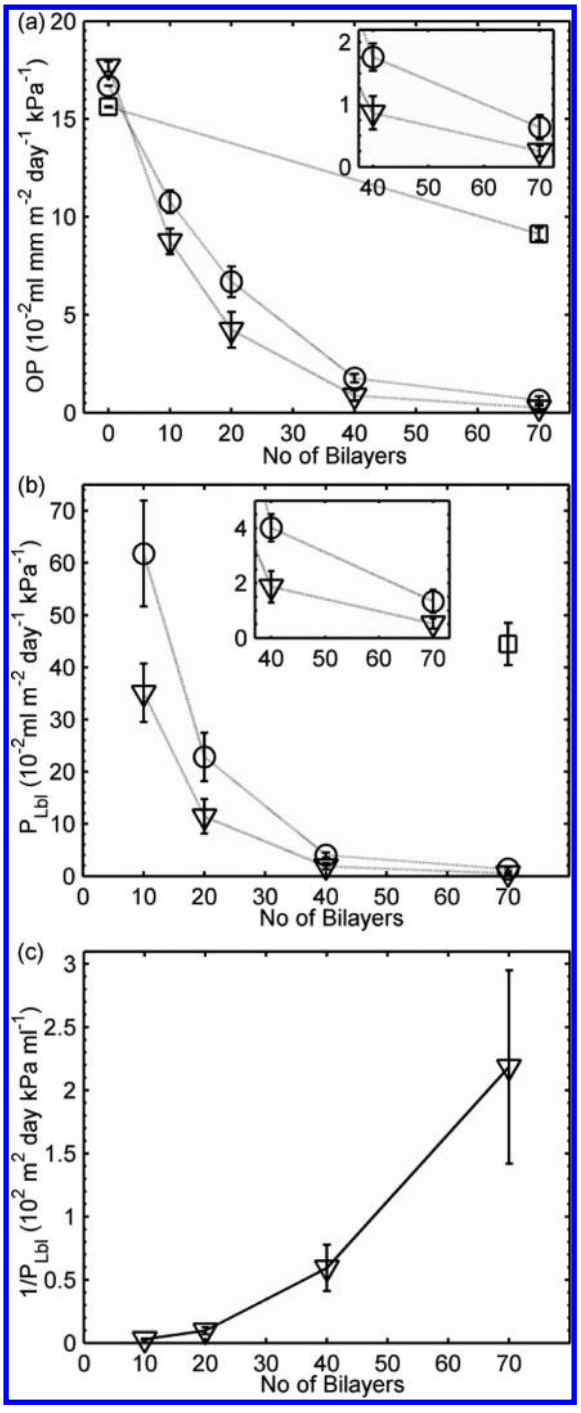

Figure 6. (a) Oxygen permeability coefficient (OP) of PLA films coated with varying numbers of MMT/chitosan bilayers (0, 10, 20, 40 and 70) obtained at 20 (∇), 50 (○), and 80% RH (□). The average film thickness was 495 ± 8 μm. (b) Oxygen permeance of multilayer coatings (P_{Lbl}) at 20 (∇), 50 (○), and 80% RH (□). The P_{Lbl} values were calculated from data in panel a using eq 3. (c) Reciprocal values of P_{Lbl} obtained at 20% RH (∇) in panel b. Inserts in panels a and b show higher magnification images of data obtained at 40 and 70 bilayers (20 and 50% RH). All measurements were performed at 23 °C. Lines are added as guides to the eye.

demonstrate at most 60% reduction in OP at clay addition levels of 5−10 wt % (0% RH, 23−25 °C).[8,9] Herein, we observe a 95 and 90% reduction in OP at 20 and 50% RH, respectively, for PLA films coated with 40 bilayers of MMT/chitosan, which corresponds to a total clay content as low as

~0.1 wt % (estimated from TEM and QCM-D results). Note that this clay content is substantially lower than that needed for conventionally processed PLA/clay nanocomposites to reach high oxygen barrier properties. From the viewpoint of food packaging, these multilayer-coated films are promising high-barrier materials because a material is considered to possess an adequate oxygen barrier if the OP is $<1 \times 10^{-2}$ mL mm m^{-2} day^{-1} kPa^{-1}.[44] The results reinforce the potential of the Lbl technique, which permits tailoring of multilayer coatings with nanometer-scale precision. However, the success in oxygen barrier properties is not only caused by a geometrical blocking effect due to a brick-wall structure consisting of wide impermeable clay platelets but also believed to be attributed to a compact layer structure of the adsorbed chitosan obtained under given processing conditions (pH 6 of the chitosan solution)[30] combined with strong MMT/chitosan molecular interaction through electrostatic forces and hydrogen bonding.[45] The high clay levels in the multilayer coatings present an extraordinarily large clay surface area, which may have a profound effect on the barrier properties.[19,20] For example, if there is poor polymer chain packing adjacent to the clay surfaces, this could lead to increased free volume for the interfacial polymer and thus higher oxygen permeance in these regions. This might effectively lower the overall barrier properties of the multilayer coating.[19] Equally, strong polymer−clay interaction is important because it allows the clay to bond to the adjacent polymer, thereby reducing the polymer mobility and thus making it more difficult for oxygen to penetrate the interfacial polymer layers.[20]

In Figure 6a, the OP at 80% RH is also included for neat PLA (15.63×10^{-2} mL mm m^{-2} day^{-1} kPa^{-1}) and a PLA film with 70 bilayers of MMT/chitosan. In this case, the OP decrease is only 42%; however, this OP value could potentially be lowered by increasing the number of bilayers or laminating a protective hydrophobic layer to the surface.[21] In comparison, multilayer coatings consisting of MMT/PAM prepared by Grunlan et al. showed much better oxygen barrier properties at high relative humidities.[21] The reduced barrier effect of the multilayer coating at high relative humidity may be attributed to the plasticizing effect of water on chitosan. For polysaccharides, in general, the good oxygen barrier properties can be explained by strong intra- and intermolecular hydrogen bonding. However, water disrupts these bonds and OP rapidly increases at RH values above 70%.[46] Alternatively, the presence of water could interfere with the molecular interaction between chitosan and MMT, with increased segmental mobility of the chitosan (increased free volume) in the interfacial areas.

In Figure 6b, the oxygen permeance data for the multilayer coating, P_{Lbl}, is presented. These data were calculated from the OP coefficients reported in Figure 6a using eq 3. Again, an extraordinary reduction in permeance is detected with elevated numbers of bilayers at 20 and 50% RH. At 40 bilayers and 20% RH, the P_{Lbl} is 1.86×10^{-2} mL m^{-2} day^{-1} kPa^{-1}. As observed by TEM, the thickness of this coating is 205 nm on each side of the PLA film. On the basis of these data, the OP coefficient for the multilayer coating, OP_{Lbl}, can be calculated and compared with that retrieved by Grunlan et al. for a multilayer MMT/PEI structure at 0% RH and 23 °C.[22] Therein, the OP_{Lbl} is always calculated for multilayers deposited on one side of a double-sided coated PET film and we therefore processed our data accordingly. For 20 bilayers of MMT/chitosan, present on one side of the PLA film, the OP_{Lbl} is 0.763×10^{-5} mL mm m^{-2} day^{-1} kPa^{-1}. This value is very close to that of 0.546×10^{-5} mL mm m^{-2} day^{-1} kPa^{-1} reported for 20 bilayers of MMT/PEI on PET.[22] The difference in OP_{Lbl} values might be explained by the use of different OTR testing equipment and/or methods for measuring the multilayer thickness in the two studies. The multilayer thickness was measured using TEM in the present article, whereas the ellipsometry technique was used by Grunlan et al.

The oxygen permeance data reported in Figure 6b for the multilayer coatings can also be compared with the barrier properties of a single layer coating containing about the same amount of chitosan and clay as the sum of all multilayers to illustrate the importance of deposition technique on oxygen barrier properties. Vartiainen et al. applied a ~1 μm thick single layer coating using the standard coating bar no. 6.[47] The coating contained 67 wt % clay and was applied onto LDPE-coated paper. The oxygen transmission rates for the coated films and the substrate were measured at 23 °C and 0, 50 and 80% RH. Using these data and eq 3, it is possible to retrieve the oxygen permeance data for the single-layer coatings. The calculated values were 143×10^{-2} mL m^{-2} day^{-1} kPa^{-1} (0% RH), 260×10^{-2} mL m^{-2} day^{-1} kPa^{-1} (50% RH), and 3548×10^{-2} mL m^{-2} day^{-1} kPa^{-1} (80% RH). These data are significantly larger than those reported in Figure 6b at all relative humidities illustrating that multilayer coatings possess much better oxygen barrier properties; for example, compare the calculated single layer values with the data for multilayer coatings with 40 (thickness 410 nm) or 70 bilayers (<1 μm).

Because the reciprocal of the permeance (signifying barrier or resistance) is additive when constructing multilayer films, a plot of $1/P_{Lbl}$ as a function of the number of bilayers will reflect the contribution of each individual added bilayer to the overall oxygen barrier, as seen in eq 3 and Figure 6c. If all bilayers contribute equally to the oxygen barrier, then $1/P_{Lbl}$ will be a simple linear function of the number of bilayers. However, Figure 6c reveals a nonlinear accelerating growth showing that in comparison with the first bilayers closer to the PLA film surface the outer and last deposited bilayers contribute significantly more to the oxygen barrier. The building of a multilayer structure is therefore accompanied by an accelerating increase in oxygen barrier properties. The underlying mechanism is not fully understood but could comprise of greater thickness of outer layers, a sealing effect of the later bilayers on the inner bilayers, or an overall reorganization into a more densely packed structure by interlayer penetration as bilayers are deposited. This acceleration effect would need to be considered when tuning the barrier properties of the films by selecting the appropriate number of bilayers.

PLA has moderate WVP properties, and improvements are needed to compete with PET.[48] The WVPs for the multilayer-coated PLA films and neat PLA were evaluated at 37.9 ± 0.1 °C. For neat PLA, the WVP was measured to be 1.12 ± 0.014 g mm m^{-2} day^{-1} kPa^{-1}. As the number of bilayers increased, a slight decrease in WVP was detected, with a value of 0.90 ± 0.024 g mm m^{-2} day^{-1} kPa^{-1} recorded when 70 bilayers of MMT/chitosan were applied. The lack of a larger improvement could be due to the hydrophilic nature of chitosan and reduced chitosan−clay interaction at the interface due to the presence of water, both of which could enhance the water vapor permeance. Chitosan films have a high WVP of 25.5 g mm m^{-2} day^{-1} kPa^{-1} at 37.8 and 90% RH as reported in the literature, which is much higher than typical WVP values reported for PLA films.[49] These findings point to the well-established fact that often a combination of two different materials is needed to obtain

dx.doi.org/10.1021/bm201438m | Biomacromolecules 2012, 13, 397−405

films with both high oxygen and water barrier properties. An example of this is commercial laminated films of polyethylene (PE) and ethylene vinyl alcohol copolymer (EVOH), in which EVOH and PE, respectively, have excellent oxygen barrier and water barrier properties.

CONCLUSIONS

Very thin laminar multilayer structures of chitosan and MMT clay were assembled due to mainly electrostatic forces on PLA films using simple Lbl processing steps. The resulting multilayer-coated PLA films had high optical clarity and showed significantly increased oxygen barrier properties. Compared with uncoated PLA, PLA films coated with 70 bilayers of MMT/chitosan had an OP that was almost two orders of magnitude lower at 20% RH (23 °C) and more than one order of magnitude lower at 50% RH (23 °C). The data correspond to better oxygen barrier properties than PET at these humidities. At 80% RH, the MMT/chitosan coating approach was less effective, which may be due to increased free volume effects in the chitosan layers in the presence of plasticizing water.

The effective oxygen barrier provided at 20 and 50% RH by the multilayer MMT/chitosan coating may be attributed to several factors: (1) enhanced exfoliation of clay platelets by subjecting the MMT suspension to a high-pressure homogenization step, (2) the well-defined "brick-wall" structure of impermeable MMT in the coating as seen by QCM-D and TEM, (3) strong MMT-chitosan molecular interaction or good chitosan chain packing adjacent to the clay surface in the multilayer structure, and (4) possible reorganization mechanisms during Lbl assembly, which allow outer layers to contribute more to the oxygen barrier properties.

In contrast with the oxygen barrier effect, the WVP was reduced by only 20% when 70 MMT/chitosan bilayers were applied. Future research aimed at further reductions in the WVP and the OP of multilayer-coated PLA films at high humidities might involve increasing the number of bilayers, cross-linking the chitosan or laminating the surface with a protective PLA film or a more hydrophobic film layer.

ACKNOWLEDGMENTS

We wish to acknowledge support for this work through the NanoPack project funded by the Danish Strategic Research Council. The assistance of Professor P. Hyttel, laboratory technician. H. M. Mølbak Holm (University of Copenhagen, Denmark), and Dr. L. Fogelström (Royal Institute of Technology, Sweden) with TEM imaging is also gratefully acknowledged.

REFERENCES

(1) Inkinen, S.; Hakkarainen, M.; Albertsson, A. C.; Sodergard, A. *Biomacromolecules* **2011**, *12*, 523−532.
(2) Drumright, R. E.; Gruber, P. R.; Henton, D. E. *Adv. Mater.* **2000**, *12*, 1841−1846.
(3) Auras, R. A.; Harte, B.; Selke, S.; Hernandez, R. *J. Plast. Film Sheeting* **2003**, *19*, 123−135.
(4) Isogai, A.; Fukuzumi, H.; Saito, T.; Wata, T.; Kumamoto, Y. *Biomacromolecules* **2009**, *10*, 162−165.
(5) Drieskens, M.; Peeters, R.; Mullens, J.; Franco, D.; Lemstra, P. J.; Hristova-Bogaerds, D. G. *J. Polym. Sci., Part B: Polym. Phys.* **2009**, *47*, 2247−2258.
(6) Sanchez-Garcia, M.; Lagaron, J. *Cellulose* **2010**, *17*, 987−1004.
(7) de Azeredo, H. M. C. *Food Res. Int.* **2009**, *42*, 1240−1253.
(8) Chang, J. H.; An, Y. U.; Sur, G. S. *J. Polym. Sci., Polym. Phys.* **2003**, *41*, 94−103.
(9) Chowdhury, S. R. *Polym. Int.* **2008**, *57*, 1326−1332.
(10) Na, H. S.; Kim, S. C. *J. Macromol. Sci., Part A* **2010**, *47*, 254−264.
(11) Cussler, E. L.; Hughes, S. E.; Ward, W. J.; Aris, R. *J. Membr. Sci.* **1988**, *38*, 161−174.
(12) Rhim, J. W.; Hong, S. I.; Ha, C. S. *LWT−Food Sci. Technol.* **2009**, *42*, 612−617.
(13) Ray, S. S.; Okamoto, M. *Prog. Polym. Sci.* **2003**, *28*, 1539−1641.
(14) Podsiadlo, P.; Kaushik, A. K.; Arruda, E. M.; Waas, A. M.; Shim, B. S.; Xu, J. D.; Nandivada, H.; Pumplin, B. G.; Lahann, J.; Ramamoorthy, A.; Kotov, N. A. *Science* **2007**, *318*, 80−83.
(15) Podsiadlo, P.; Tang, Z. Y.; Shim, B. S.; Kotov, N. A. *Nano Lett.* **2007**, *7*, 1224−1231.
(16) Podsiadlo, P.; Michel, M.; Lee, J.; Verploegen, E.; Kam, N. W. S.; Ball, V.; Lee, J.; Qi, Y.; Hart, A. J.; Hammond, P. T.; Kotov, N. A. *Nano Lett.* **2008**, *8*, 1762−1770.
(17) Decher, G. *Science* **1997**, *277*, 1232−1237.
(18) Li, Y. C.; Schulz, J.; Grunlan, J. C. *ACS Appl. Mater. Interfaces* **2009**, *1*, 2338−2347.
(19) Xue, L. P.; Borodin, O.; Smith, G. D. *J. Membr. Sci.* **2006**, *286*, 293−300.
(20) Hedenqvist, M. S.; Backman, A.; Gallstedt, M.; Boyd, R. H.; Gedde, U. W. *Compos. Sci. Technol.* **2006**, *66*, 2350−2359.
(21) Jang, W. S.; Rawson, I.; Grunlan, J. C. *Thin Solid Films* **2008**, *516*, 4819−4825.
(22) Priolo, M. A.; Gamboa, D.; Grunlan, J. C. *ACS Appl. Mater. Interfaces* **2010**, *2*, 312−320.
(23) Priolo, M. A.; Gamboa, D.; Holder, K. M.; Grunlan, J. C. *Nano Lett.* **2010**, *10*, 4970−4974.
(24) Hunter, A. C. *Adv. Drug Delivery Rev.* **2006**, *58*, 1523−1531.
(25) Woodrow, J. E.; Seiber, J. N.; Miller, G. C. *J. Agric. Food Chem.* **2008**, *56*, 2773−2779.
(26) Wang, X.; Du, Y.; Luo, J. *Nanotechnology* **2008**, *19*, 065707.
(27) Kumar, M. N. V. R. *React. Funct. Polym.* **2000**, *46*, 1−27.
(28) Annabi-Bergaya, F. *Micropor. Mesopor. Mater.* **2008**, *107*, 141−148.
(29) Ploehn, H. J.; Liu, C. Y. *Ind. Eng. Chem. Res.* **2006**, *45*, 7025−7034.
(30) Claesson, P. M.; Ninham, B. W. *Langmuir* **1992**, *8*, 1406−1412.
(31) Rodahl, M.; Hook, F.; Krozer, A.; Brzezinski, P.; Kasemo, B. *Rev. Sci. Instrum.* **1995**, *66*, 3924−3930.
(32) Sauerbrey, G. *Z. Phys.* **1959**, *155*, 206−222.
(33) Ogawa, Y.; Arikawa, Y.; Kida, T.; Akashi, M. *Langmuir* **2008**, *24*, 8606−8609.
(34) Dahneke, B. *Measurements of Suspended Particles by Quasi-Elastic Light Scattering*; Wiley-Interscience: New York, 1983.
(35) Jiao, Y. H.; Li, Y.; Wang, S.; Zhang, K.; Jia, Y. G.; Fu, Y. *Langmuir* **2010**, *26*, 8270−8273.
(36) Svensson, O.; Lindh, L.; Cárdenas, M.; Arnebrant, T. *J. Colloid Interface Sci.* **2006**, *299*, 608−616.
(37) Aulin, C.; Johansson, E.; Wågberg, L.; Lindström, T. *Biomacromolecules* **2010**, *11*, 872−882.
(38) Aulin, C.; Varga, I.; Claesson, P. M.; Wågberg, L.; Lindström, T. *Langmuir* **2008**, *24*, 2509−2518.
(39) Park, S. J.; Lee, K. Y.; Ha, W. S.; Park, S. Y. *J. Appl. Polym. Sci.* **1999**, *74*, 2571−2575.
(40) Bergaya, F.; Theng, B. K. G.; Lagaly, G. *Handbook of Clay Science*; Elsevier: Amsterdam, 2006.
(41) Hensen, E. J. M.; Smit, B. *J. Phys. Chem. B* **2002**, *106*, 12664−12667.
(42) Hong, S. I.; Lee, J. H.; Bae, H. J.; Koo, S. Y.; Lee, H. S.; Choi, J. H.; Kim, D. H.; Park, S.-H.; Park, H. J. *J. Appl. Polym. Sci.* **2011**, *119*, 2742−2749.
(43) Crank, J. *Mathematics of Diffusion*; Clarendon Press: Oxford, U.K., 1967.
(44) Edlund, U.; Ryberg, Y. Z.; Albertsson, A. C. *Biomacromolecules* **2010**, *11*, 2532−2538.

(45) Paluszkiewicz, C.; Stodolakb, E.; Hasik, M.; Blazewicz, M. *Spectrochim. Acta, Part A* **2011**, *79*, 784−788.
(46) Aulin, C.; Gallstedt, M.; Lindstrom, T. *Cellulose* **2010**, *17*, 559−574.
(47) Vartiainen, J.; Tuominen, M.; Nättinen, K. *J. Appl. Polym. Sci.* **2010**, *116*, 3638−3647.
(48) Auras, R. A.; Singh, S. P.; Singh, J. J. *Packag. Technol. Sci.* **2005**, *18*, 207−216.
(49) Oguzlu, H.; Tihminlioglu, F. *Macromol. Symp.* **2010**, *298*, 91−98.